Journal of Alloys and Compounds 509 (2011) 10121–10126

Contents lists available at ScienceDirect

Journal of Alloys and Compounds

journal homepage: www.elsevier.com/locate/jallcom

Anatase TiO_2 sols derived from peroxotitanium acid and to form transparent TiO_2 compact film for dye-sensitized solar cells

Difeng Qian [a], Yaogang Li [b], Qinghong Zhang [b,*], Guoying Shi [c], Hongzhi Wang [a,*]

[a] State Key Laboratory for Modification of Chemical Fibers and Polymer Materials, Donghua University, Shanghai 201620, PR China
[b] Engineering Research Center of Advanced Glasses Manufacturing Technology, MOE, Donghua University, Shanghai 201620, PR China
[c] College of Chemistry, Chemical Engineering and Biotechnology, Donghua University, Shanghai 201620, PR China

ARTICLE INFO

Article history:
Received 4 April 2011
Received in revised form 9 August 2011
Accepted 9 August 2011
Available online 19 August 2011

Keywords:
Peroxotitanium acid
Compact film
Gradient layer
Dye-sensitized solar cell
Titania

ABSTRACT

Transparent and surfactant-free TiO_2 sols containing anatase nanocrystals were prepared by the hydrothermal treatment of water-soluble peroxotitanium acid (PTA) at a temperature of 120 °C. The TiO_2 nanocrystals were characterized by transmission electron microscopy (TEM). The TEM results indicated that the TiO_2 nanocrystals were nanorod-like with diameters of less than 7 nm after the subsequently hydrothermal treatment. A gradient layer between the transparent fluorine doped SnO_2 (FTO) layer and the porous titanium dioxide nanocrystalline film for dye-sensitized solar cells (DSSCs) photoelectrodes, was made with the as-prepared TiO_2 sols. The TiO_2 gradient layers were characterized by field-emission scanning electron microscopy and UV–vis absorption spectrometry. After the gradient layer deposition on the FTO coated glass, the composite multilayer film exhibited the visible light transmittance of 80% which approached to that of bare FTO glass. The photo-to-electric energy conversion efficiency of the N719 dye-sensitized solar cell had significantly improved from 4.2% to 5.6% in the presence of the compact layer between FTO and the porous TiO_2 nanocrystalline film under of AM1.5 illumination (100 mW/cm^2). The remarkable improvements in short-circuit current for the DSSCs was due to the effective gradient layer at the FTO–TiO_2 interface which prevented direct contact of electrolytes with FTO and consequently reduced charge recombination losses.

1. Introduction

Dye-sensitized porous nanocrystalline TiO_2 solar cells (also known as Grätzel cells) have received considerable attention for their potential as a cost-effective alternative to silicon solar cells [1–10]. Typical dye-sensitized solar cells (DSSCs) comprise nanocrystalline TiO_2 photoelectrodes, dye molecules, redox shuttle electrolytes and counter electrodes. The photoelectrode is one of main factor in determining the performance of DSSCs [11–15]. A typical photoanode application for DSSCs commonly consists of a porous TiO_2 layer coated on a conducting substrate (e.g. fluorine-doped tin oxide, FTO) with the adsorbed sensitized dye at the TiO_2 surface [11]. The porous TiO_2 layer essentially serves the purpose of collecting and transporting photoelectrons injected by the photoexcited dye via the TiO_2 conduction band to the conducting substrate, and then to the external circuit. However, a nanocrystalline TiO_2 film can lead to the formation of some voids between the TiO_2 nanoparticles and the FTO glass interface, decreasing the open circuit voltage (V_{oc}) by the electron back-transport reaction, also known as "electron leakage" [16–18]. The existence of holes in the photoelectrode also makes it possible for the electrolyte to contact directly with the conductive substrate. In solid-state cells, it has been demonstrated that the FTO substrates must be covered by a thin blocking layer of titanium dioxide in order to prevent efficiency loss due to electron transfer to the hole-conducting medium from the FTO [19]. Also, dye layers located at the FTO-electrolyte interface can potentially increase recombination by acting as a catalyst to promote the two-electron reduction step from triiodide (I_3^-) to iodide (I^-) [20]. Therefore, controlling the interface between the FTO and nanocrystalline TiO_2 layers is essential for the formation of efficient DSSCs. Usually, a dilute $TiCl_4$ solution is used to deposit a compact film on the surface of the conductive substrate prior to coating with the porous TiO_2 film [21]. The compact layer physically blocks the reaction of the photo-injected electrons and the I_3^- ions at the FTO/electrolyte interface. Such a compact film cannot only separate the electrolyte from the substrate, but also improve the adhesion of the porous TiO_2 film. The compact film also refers to the blocking film or the passivating layer in the literatures [19,22], but the compact film is popularly used due to it has a more dense structure compared to the porous TiO_2 film.

* Corresponding authors. Tel.: +86 21 67792943; fax: +86 21 67792855.
E-mail addresses: zhangqh@dhu.edu.cn (Q. Zhang), wanghz@dhu.edu.cn (H. Wang).

0925-8388/$ – see front matter © 2011 Elsevier B.V. All rights reserved.
doi:10.1016/j.jallcom.2011.08.055

Recent studies showed an improvement in the cell's efficiency after the use of the blocking layer [23–32]. Blocking layers of Nb_2O_5 [25–28], ZnO [29–31], TiO_2 [31–34], Au [35], graphene oxide and TiO_2 nanocomposites [36] were deposited by different methods such as spray pyrolysis, dip-coating, spin-coating and layer-by-layer [6]. For example, Yanagida and co-workers [25,26] studied thin Nb_2O_5 and TiO_x blocking layers between FTO and a porous TiO_2 layer. The improvement in performance of the DSSCs was attributed to the effective reduction of the electron loss at the FTO/porous TiO_2 interface. Cameron and Peter [33] studied the properties of thin blocking layers of titanium dioxide through electrochemical impedance spectroscopy, and showed that the ability of the blocking layer to prevent the back reaction of electrons with tri-iodide ions in the electrolyte is excellent under short circuit conditions. Very recently, Liu et al. found the ZnO compact film had some advantages over TiO_2 for improving of the short-circuit current density for DSSCs [30,31] and obtained the photoelectric conversion efficiency as high as of 7.76% in the presence of ZnO compact film. Kim et al. [36] used a mixture of graphene oxide and TiO_2 nanocomposites, which was reduced photocatalytically by UV light irradiation and applied as an interfacial layer between a FTO layer and a nanocrystalline TiO_2 film. It is believed that the two-dimensional graphene sheets decrease the direct contact of the electrolyte with the FTO substrate significantly. The photoelectric conversion efficiency (η) increased from 4.89% to 5.26% after introducing the graphene-TiO_2 interfacial layer. The improvement of the DSSCs performance has drawn many attentions recently. For example, the one-dimensional TiO_2 nanotubes and ZnO nanowires were introduced into the photoanodes of DSSCs [35,37,38], and an enhanced η was achieved respectively.

In this article, we describe a hydrothermal treatment of the water-soluble peroxotitanium acid (PTA), from which we obtained anatase TiO_2 nanorod sols with perfectly crystallized TiO_2. Transparent and surfactant-free TiO_2 anatase nanocrystalline sols were deposited on FTO glass by a dip-coating method, serving as an effective gradient layer in a photoanode. In contrast to the most commonly used amorphous TiO_2 sols derived from titanium alkoxide or dilute $TiCl_4$ solutions, the crystallites in this work were already in the anatase phase and thus did not require the further calcination at a high temperature to crystallize the amorphous TiO_2.

2. Experimental

2.1. Materials

Titanium sulfate ($Ti(SO_4)_2$, AR), hydrogen peroxide (H_2O_2, 30%, AR) and ammonia solution ($NH_3{\cdot}H_2O$, 25–28 wt%, AR) were used to make the TiO_2 sol. 4-tert-butylpyridine (Aldrich) and acetonitrile (Fluka) were purified by vacuum distillation. Guanidinium thiocyanate (Aldrich), iodine (99.999%, Aldrich), hydrogen hexachloroplatinate (IV) hydrate (H_2PtCl_6), 1,2-dimethyl-3-propylimidazolium iodide (Aldrich) and lithium iodide were used as received. Sheet glass (Nippon Sheet Glass, Hyogo, Japan) was coated with a fluorine-doped tin oxide (FTO) layer (sheet resistance of 14 Ω/□). A hot melt polymer foil (Surlyn 1702, DuPont) was used as a spacer frame between the electrode substrates. The dye N719, also known as Ruthenium 535-bisTBA (RuL2(NCS)2:2TBA, L = 2,2-bipyridyl-4,4-dicarboxylic acid, TBA = tetrabutylammonium), was purchased from Solaronix. Degussa P25 powders were provided by the Degussa Company (30% rutile and 70% anatase, mean crystallite size of 30 nm and BET specific surface area of 50 m^2/g).

2.2. Preparation of transparent TiO_2 sol and TiO_2 gradient layer

In a typical synthesis process, titanium sulfate was adjusted to 0.5 M as a stock solution with deionized water. Ammonia (2.0 M) was slowly dropped into a vigorously stirred titanium sulfate solution, which was heated in advance to 70 °C, until the solution pH value was 7. As we reported previously, the precipitates at 70 °C from a titanium salt contained mainly anatase TiO_2 in the presence of sulfate ions [39,40]. A white precipitate was formed instantaneously, and a large amount of precipitate was obtained after the ammonia solution was used up. The precipitate was collected by filtration and then washed with deionized water for several times. Subsequently, 10 g of precipitates were peptized with 60 ml of aqueous hydrogen peroxide (30%); continuous magnetic stirring was required to avoid immediate dense gel formation during dissolution and to keep the reactant mixed uniformly. The yellow, transparent and neutral PTA sol was formed after about 2 h. Finally, the PTA sol was put in an autoclave, and after hydrothermal treatment and crystallization at 120 °C for 24 h, a transparent sol containing perfect anatase crystallized TiO_2 was synthesized.

TiO_2 gradient layers using the as-prepared sol were made as follows: first, FTO glasses were cleaned by an ultrasonic treatment in ethanol and dried at 60 °C. The FTO glasses were immersed in the TiO_2 sol for 1 min to ensure that the TiO_2 sol fully covered the FTO surface. The sol modified FTO was dried in an oven at 80 °C in an air atmosphere for 10 min.

2.3. Preparation of a dye-sensitized thin film of porous TiO_2

1.0 g TiO_2 powder (Degussa P25) was first dispersed into a mixture of 5.0 ml ethanol and 3.0 ml terpineol, and sonicated for 30 min to form slurry. The slurry was coated on the compact TiO_2 layer by screen-printing, and keep same porous TiO_2 thickness (average height are 15 μm measured by surface profiler) in all films. Control samples were also produced without the compact layer. The films were heated at 450 °C for 30 min and stored in desiccators until they were used in solar cell construction.

2.4. Dye-sensitized solar cell assembly

The film was heated to 450 °C for 30 min and then cooled to room temperature. The TiO_2 coating layer film after calcination was in thickness of 15 μm. Then, the electrode was immersed for 48 h in a solution of ruthenium dye N719 at a concentration of 3.0×10^{-4} M. The electrode was then rinsed with acetonitrile to remove excess amounts of dye and dried. A hot melt polymer foil (Surlyn 1702, DuPont) was used as a spacer frame between the electrode substrates. One drop of an iodine-based electrolyte solution was deposited onto the surface of the electrode and penetrated inside the TiO_2 film by capillary action. The electrolyte solution, which was composed of 0.6 M of 1,2-di-methyl-3-propylimidazolium iodide, 0.05 M of iodine, 0.1 M of lithium iodide, and 0.5 M of tert-butylpyridine, was dissolved in acetonitrile. The components of the electrolyte were similar to those in the literature as reported by Grätzel [4]. The counter electrode was platinized by applying a drop of 0.005 M H_2PtCl_6 in 2-propanol to a FTO glass substrate, and calcined it in air at 385 °C for 15 min. Then the counter electrode was clamped on to the top of the TiO_2 working electrode. Finally, a silver paste was added on clean areas of FTO glass to enhance conductivity and ensure good contact during measurement.

2.5. Characterizations

The powder phase composition was identified by X-ray diffraction (XRD) equipment (Model D/max 2550V, Rigaku Co. Tokyo, Japan), using Cu K(((= 1.5406 Å) radiation. The broadening of the XRD peak at 2(= 25.4° (d_{101}) for anatase TiO_2 was used to calculate the crystallite size according to the well-known Scherrer formula. The morphology and size of the resultant titanium dioxide were observed using transmission electron microscopy (TEM) (JEM-2100F, JEOL Co., Japan). The UV–vis absorption spectra of the films were measured with a Lambda 35 spectrophotometer. Film morphology and thickness were characterized by field-emission scanning electron microscopy (FE-SEM) (Hitachi S-4800, Japan) and the film thickness measured by an optical profiler (Wyko NT9100, Veeco, USA). The photovoltaic properties of the solar cells were measured with a source meter (Keithley, Model 2400) under the illumination of simulated sunlight provided by an Oriel solar simulator (Model 91160) with an AM1.5 filter and a 300 W xenon lamp. The light intensity during the I/V characteristics measurement was 100 mW/cm^2 which monitored by a Newport 1918-C power meter with 818P-030-18 PWR detector head. The electrochemical impedance spectra were collected using a Zennium electrochemical workstation (Model CIMPS-1, Zahner-elecktrik GmbH & Co., Germany).

3. Results and discussion

As shown in Fig. 1(a), the dried sol contained well-crystallized anatase TiO_2 with a mean crystallite size of about 7.4 nm on the basis of the calculation with Scherrer formula. As reported in the JCPDS No. 21-1272, the relative intensity of the (0 0 4) plane to the (2 0 0) plane was 20/35. However, for the TiO_2 sols obtained from the hydrothermal treatment of water-soluble peroxotitanium acid (PTA), the relative intensity of (0 0 4) to (2 0 0) was changed to 38/28. This result suggested that the oriented attachment in anatase titania occurred occasionally on the (0 0 1) plane, which resulted from the reduction of the overall surface energy by the elimination of the surface area where the crystallites joined [41].

TEM micrographs of TiO_2 nanocrystals in the sol were given in Fig. 1(b) and (c). Most of the nanoparticles had elongated rod-like morphologies, and they were connected to each other to form a network shape. Almost no spherical crystallites were observed, and the

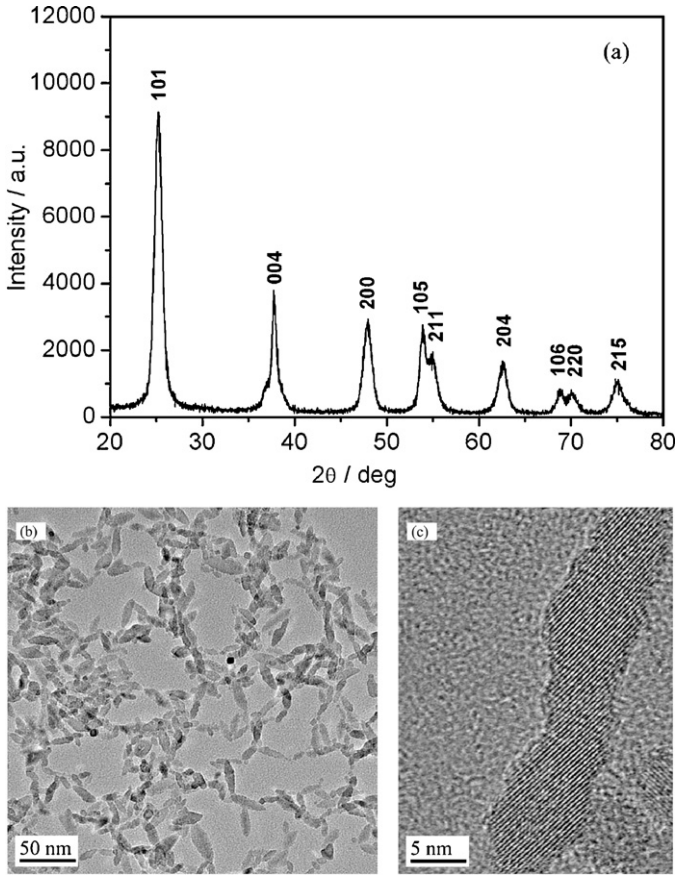

Fig. 1. (a) XRD pattern of the dried sol of TiO_2 sample, (b) TEM images of TiO_2 sol, and (c) high-resolution TEM image of TiO_2 rod-like nanocrystals along the *c* axis with the exposed (0 0 2) plane.

rod-like nanocrystals had a diameter of about 7 nm. It was noted that these rod-like nanocrystals were not of uniform diameter, but instead possessed a zigzag diameter. As shown in the high-resolution TEM (HRTEM) image (Fig. 1(c)), which was typical for the nanorods formed by the oriented attachment (OA) mechanism [42].

The deposition of the TiO_2 sol compact layer on the FTO substrate was monitored by UV–vis spectroscopy, and the transmittance spectra of both bare FTO substrates and those with the deposited compact film are presented in Fig. 2. After deposited by the TiO_2 sol compact layer, the FTO remained the same transmittance to that of the bare one in the visible light region. It was necessary for the compact TiO_2 films on substrates to retain primary transparency in order to improve light harvesting efficiency. Light passed through the titanium dioxide gradient layer and the absorption of light by the dye was uninfluenced. The transmittance of the compact films was more than 80% in the visible light region and an onset of 380 nm was obtained due to the intrinsic absorption of TiO_2 in the ultraviolet region. There was no significant difference in the UV–vis transmission spectra of the films prepared by the TiO_2 sols in two concentrations, one of 2.718 g/l and another of 1.359 g/l. This allowed the surfactant-free TiO_2 sols to readily cover the FTO surface. The characteristics of low viscosity and rapid solvent evaporation enabled the formation of a dense and uniform thin film on the FTO surface. The thin coating layer was therefore not expected to change the transmittance (or did not affect the dye light harvesting efficiency) of the original FTO surface.

The surface morphology and cross-sectional images of the electrodes were observed by field-emission scanning electron

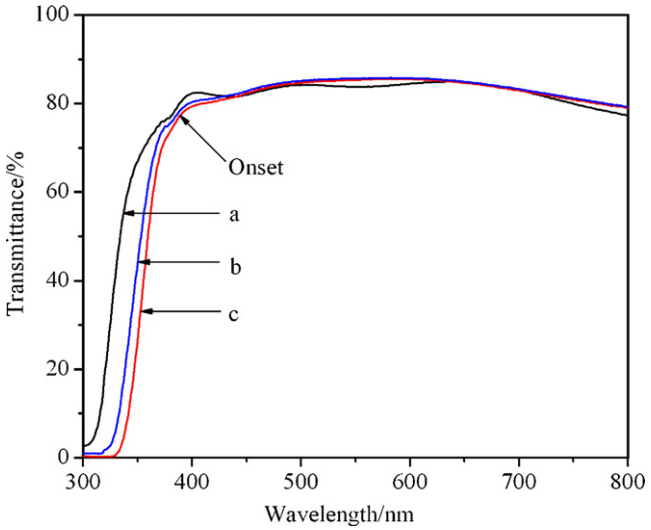

Fig. 2. UV–vis transmittance spectra of (a) bare FTO substrate, and FTO glass coated with TiO_2 sols with varying concentrations of (b) 2.718 g/l and (c) 1.359 g/l.

microscopy (FE-SEM). Fig. 3(a) showed images of the bare FTO surface. It could be seen that the gradient layers were uniform and dense, and that the particle size was about 30 nm from Fig. 3(b). As-prepared TiO_2 sol with small nanoparticles could be more efficiently packed on to the substrate surface, since voids among the particles were reduced as their size decreases [24]. Fig. 3(c) showed an image of the surface morphology of a porous TiO_2 layer. Fig. 3(d) showed the cross-sectional image of the compact layer with a thickness of 2 μm and a porous layer on the FTO substrate.

As mentioned earlier, a thick TiO_2 layer formed by the doctor blade or screen-printing methods could not cover the rough FTO surface uniformly. Iodide (I^-) ions in the electrolyte could migrate from the counter electrode to the nanoporous layer of TiO_2, transfer the electrons to the highest occupied molecular orbital level of the dye adsorbed on TiO_2, and then be converted to triiodide (I_3^-) ions. Some of the I_3^- ions in the electrolyte penetrated the porous TiO_2 and could directly contact the FTO surface, thereby collecting electrons from the FTO surface through the back-transport reaction [21]. As shown in Fig. 4, the presence of the TiO_2 compact layer between FTO and the porous TiO_2 layer in the DSSCs might inhibit the direct contact between I_3^- ions and the FTO layer, effectively prevent the back-transport of electrons from the FTO layer to the I_3^- ions [29], and cause the increase of the short-circuit current. It could be stated that the back-transport of electrons from the FTO electrode to the I_3^- ions was suppressed by the introduction of the gradient TiO_2 layer [26]. The uniform and dense gradient TiO_2 layer acted as a barrier between the FTO layer and the electrolyte.

The electrochemical impedance spectroscopy was used to study the interfacial layer electron recombination resistance. Fig. 5 showed the Nyquist plots of the DSSCs employing the bare FTO and the sol treated FTO substrates. Two semicircles were observed in the measured frequency rang of 10^{-1} to 10^5 Hz for both two electrodes. According to previous analysis [25], low frequency and high frequency regions were attributed to impedance related to charge transfer processes occurring at the FTO–TiO_2/dye/electrolyte interface and Pt/electrolyte interface, respectively. The second semicircle of the TiO_2 sol treated DSSC was larger than that obtained from in the absence of TiO_2 sol compact film one, which indicated that the charge transported at the FTO/TiO_2 interface at the present was more difficult compared to no compact layer electrode. Charge-transfer resistance in the electrode with the presence of 1 μm gradient layer appeared to be bigger than that of electrode in the absence of gradient layer, as

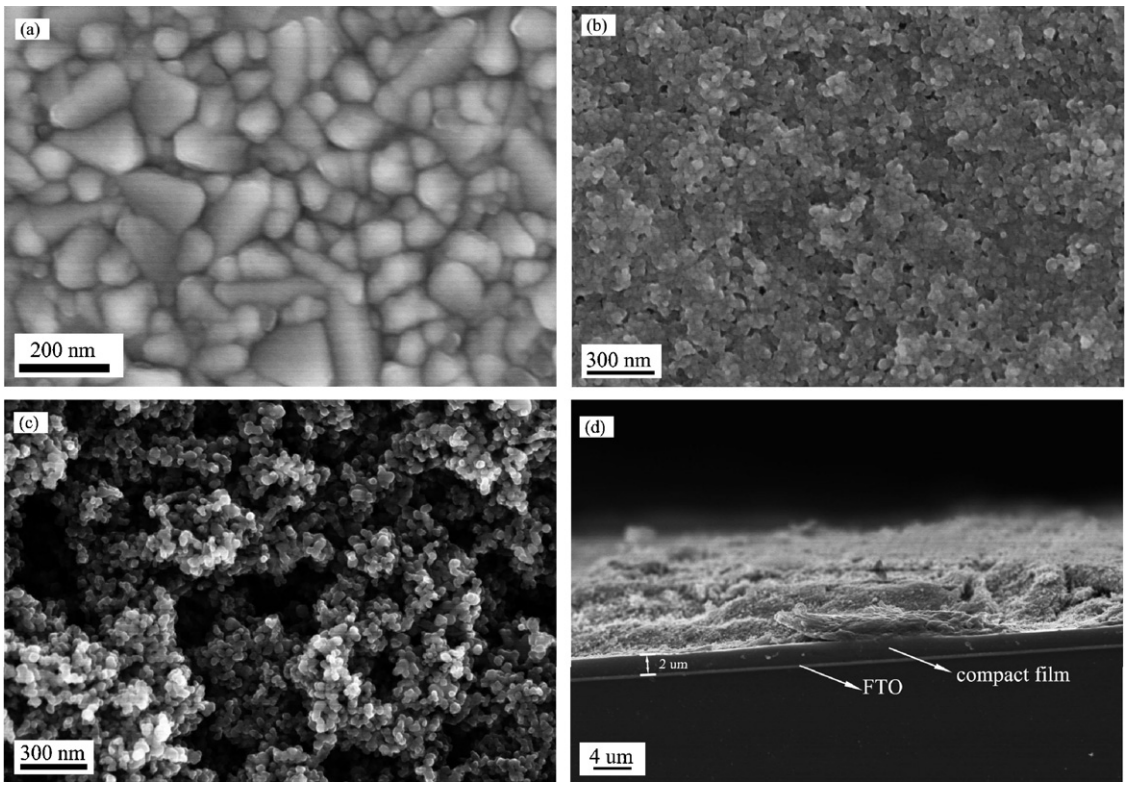

Fig. 3. FE-SEM surface images of (a) bare FTO and (b) TiO_2 sol with concentration of 2.718 g/l coated on FTO, (c) porous TiO_2 layer, and (d) cross-sectional images of the final TiO_2 electrode.

shown in Fig. 5. It was explained that the back-transport of electrons from the FTO electrode to the I_3^- ions was suppressed by the introduction of TiO_2 compact film. During the deposition Pt as a counter electrode, there were some slight differences such as the Pt crystallites contacting and the thickness of Pt layer between the counter electrodes. These differences caused that the resistance for these two cells in the high frequency was inconsistent. However, minor difference of the high frequency impedance had little effect on overall cell efficiency. In addition, the electrolyte diffusion coefficient of the sol treated DSSC in the region became smaller, and then the corresponding resistance of Nernstian diffusion in electrolyte became larger.

The N719-sensitized TiO_2 solar cells were characterized by measuring their current–voltage behavior using a black metal mask with an aperture area of 0.64 cm^2 under standard AM1.5 simulated sunlight (power density of 100 mW/cm^2). Fig. 6 showed the typical current density versus voltage curves of the DSSCs with and without the gradient layer. It was clear that the DSSC without the gradient layer performed comparatively poorly, and there was a significant increase in current density and open-circuit voltage for the DSSCs with the gradient layer, as shown in Table 1. A light-to-electricity conversion efficiency of 5.6% was obtained for the DSSC with the incorporation of a blocking layer, whereas the DSSC without a compact layer only attained efficiency of 4.2%.

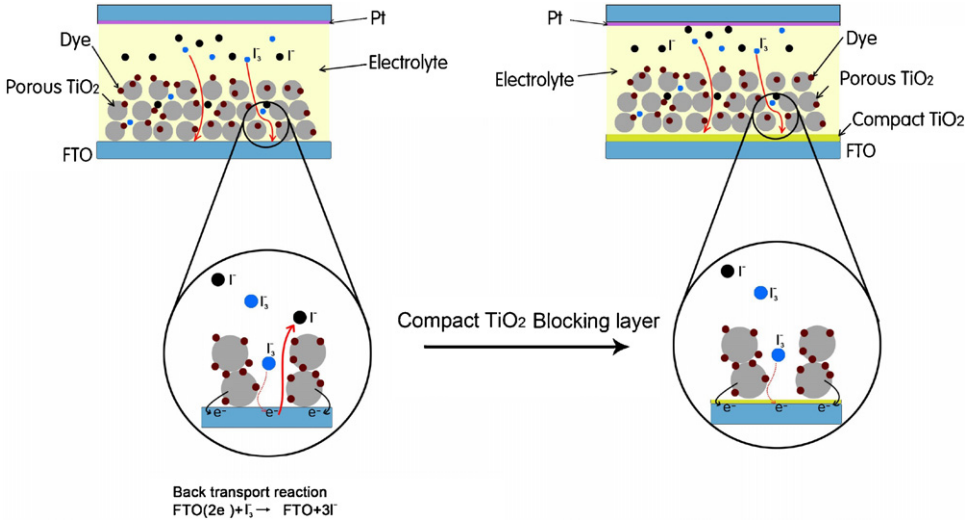

Fig. 4. Schematic representation and mechanism of applied transparent TiO_2 sol as efficient blocking layer to prevent the back-transport reaction of electrons.

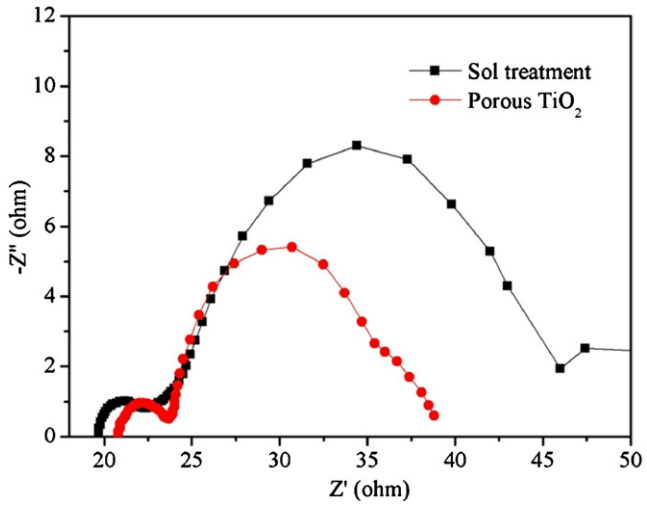

Fig. 5. Nyquist plots of the DSSCs employing the bare FTO and the sol treated FTO substrates measured under an illumination of 100 mW/cm^2. After the sol treatment, the gradient layer in thickness of 1 μm was formed.

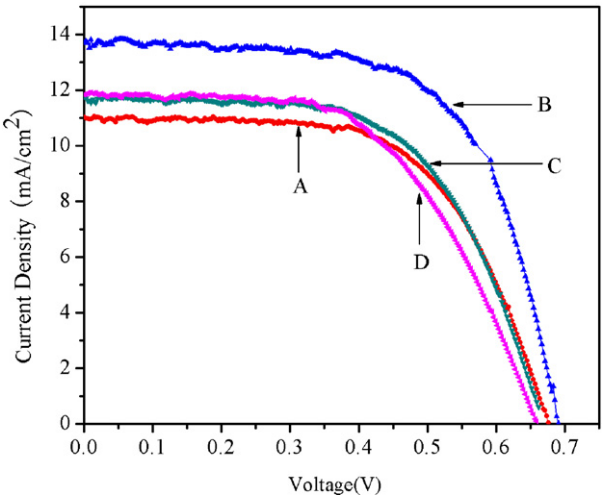

Fig. 6. Illustration of the *J–V* characteristics curves of the DSSCs with and without compact TiO_2 layers. A: TiO_2 nanocrystalline porous film without gradient layer, B, C and D: TiO_2 nanocrystalline porous film with gradient layers in thickness of 1 μm, 2.5 μm, 4 μm, respectively.

The thickness of compact layer was depended on the concentration of TiO_2 sol and the number of dip-coating. Fig. 6 also showed the current and voltage properties of the DSSCs with different thickness of the compact films, the thickness had a great impact on short-circuit current of DSSCs, but little effect on open-circuit voltage and fill factor. When the thickness of the compact layer was 1 μm, the short-circuit current of the corresponding DSSC was 13.68 mA/cm^2 and it also received the highest photoelectric conversion efficiency of 5.6%. Short-circuit current was characterized by the number of electrons flowing through the external circuit, with proportionally the number of the light generated electron arriving to photocathode. Therefore, introducing TiO_2 compact layer in an optimized thickness reduced the electron leakage and more electrons could be collected by the conductive substrate. Increasing the thickness of the compact layers, the photoelectric conversion efficiency of the DSSCs was slightly reduced. While too thick compact layers with low porosity might affect the diffusion of electrolyte, increase electron transmission path, and cause DSSC photoelectric performance down. In our experimental conditions, 1 μm thickness of compact layer was the best. Fig. 6 also showed the V_{oc} increased by introducing compact TiO_2 gradient layer in the DSSCs. The back-transport of electrons from the FTO electrode to the I_3^- ions was suppressed by the introduction of compact layer. Compact TiO_2 acted a barrier between FTO and electrolyte and thus resulted in the increase of the V_{oc}.

Table 1
Photovoltaic performance of DSSCs with four types of TiO_2 electrode.

Cell type	J_{sc} (mA/cm^2)	V_{oc} (V)	FF	η (%)
A	11.01	0.67	0.58	4.2 ± 0.1
B	13.68	0.69	0.60	5.6 ± 0.1
C	11.75	0.66	0.59	4.5 ± 0.1
D	11.84	0.65	0.57	4.4 ± 0.1

A: TiO_2 nanocrystalline porous film without gradient layer.
B, C and D: TiO_2 nanocrystalline porous film with gradient layer in thickness of 1 μm, 2.5 μm, 4 μm, respectively.

The compact layer also was referred to gradient layer in this paper, which was with a higher transparency in the visible light region and a denser microstructure compared to the porous nanocrystalline TiO_2 films. The photoelectric conversion efficiency results of DSSCs shown in Table 1 were lower than the reported data [43,44], which might be due to the following factors. Firstly, we used P25 TiO_2 as a starting material to prepare the TiO_2 paste for the porous layer, while P25 containing rutile phase TiO_2 was not good at dye adsorption. Secondly, the porous TiO_2 layer was the insufficient connectivity between the TiO_2 particles [45], and we did not use any post treatment for the porous TiO_2 surface. As a result, photoelectron transfer within the electrodes was slow, and these aspects could be further optimized.

4. Conclusions

In summary, a dip-coating method for the formation of gradient layers consisting of crystalline TiO_2 at near room temperature over FTO had been presented. Transparent and surfactant-free TiO_2 sols were used to prepare the gradient layer between FTO and the porous TiO_2 layer for dye-sensitized solar cell photoanodes. In the presence of a 1 μm thick TiO_2 gradient layer, an increase of 2.67 mA/cm^2 for the short-circuit current density was achieved in DSSCs. The TiO_2 gradient layer blocked the direct contact between the electrolyte and the FTO substrate effectively, providing retardation of the back-transport reaction in the FTO/TiO_2 interfaces. The photoelectric conversion efficiency was increased from 4.2% to 5.6% in the presence of TiO_2 compact film in thickness of 1 μm.

Acknowledgments

This research is supported by the National Natural Science Foundation of China (no. 50772127), the Cultivation Fund of the Key Scientific and Technical Innovation Project (no. 708039) and Chinese Universities Scientific Fund.

References

[1] B. O'Regan, M. Grätzel, Nature 353 (1991) 737–740.
[2] C.G. Garcia, J.F. de Lima, N.Y. Murakami Iha, Coord. Chem. Rev. 196 (2000) 219–247.
[3] M. Grätzel, Nature 414 (2001) 338–344.
[4] M. Grätzel, J. Photochem. Photobiol. C: Photochem. Rev. 4 (2003) 145–153.
[5] K. Hara, M. Kurashige, Y. Dan-Oh, C. Kasada, A. Shinpo, S. Suga, K. Sayama, H. Arakawa, New J. Chem. 27 (2003) 783–785.
[6] L. Zhang, A.J. Xie, Y.H. Shen, S.K. Li, J. Alloys Compd. 505 (2010) 579–583.
[7] M.D. Wei, Y. Konishi, H.S. Zhou, M. Yanagida, H. Sugihara, H. Arakawa, J. Mater. Chem. 16 (2006) 1287–1293.
[8] Y.J. Chena, M.C. Hsu, Y.C. Cai, J. Alloys Compd. 490 (2010) 493–498.
[9] S. Mahshid, M. Askari, M. Sasani Ghamsari, N. Afsharc, S. Lahuti, J. Alloys Compd. 478 (2009) 586–589.
[10] S. Anandan, Sol. Energy Mater. Sol. Cells 91 (2007) 843–846.
[11] C.M. Chen, Y.C. Hsu, S.J. Cherng, J. Alloys Compd. 509 (2011) 872–877.

[12] J.T. Kim, S.H. Kim, Sol. Energy Mater. Sol. Cells 95 (2011) 336–339.
[13] S. Chappel, S.G. Chen, A. Zaban, Langmuir 18 (2002) 3336–3342.
[14] A. Islam, H. Sugihara, M. Yanagida, K. Hara, G. Fujihashi, Y. Tachibana, R. Katoh, S. Murata, H. Arakawa, New J. Chem. 26 (2002) 966–968.
[15] M.K. Nazeeruddin, P. Pechy, T. Renouard, S.M. Zakeeruddin, R. Humphry-Baker, P. Comte, P. Liska, L. Cevey, E. Costa, V. Shklover, L. Spiccia, G.B. Deacon, C.A. Bignozzi, M. Graetzel, J. Am. Chem. Soc. 123 (2001) 1613–1624.
[16] K. Srinivas, K. Yesudas, K. Bhanuprakash, V. Jayathirtha Rao, L. Giribabu, J. Phys. Chem. C 113 (2009) 20117–20126.
[17] G.D. Sharmaa, P. Suresha, J.A. Mikroyannidis, Synth. Met. 160 (2010) 1427–1432.
[18] H. Yu, S.Q. Zhang, H.J. Zhao, G. Will, P. Liua, Electrochim. Acta 54 (2009) 1319–1324.
[19] C.S. Karthikeyan, K. Peter, H. Wietasch, M. Thelakkat, Sol. Energy Mater. Sol. Cells 91 (2007) 432–439.
[20] B.C. O'Regan, J.R. Durrant, P.M. Sommeling, N.J. Bakker, J. Phys. Chem. C 111 (2007) 14001–14010.
[21] E. Palomares, J.N. Clifford, S.A. Haque, T. Lutz, J.R. Durrant, J. Am. Chem. Soc. 125 (2003) 475–482.
[22] J.A. Jeong, H.K. Kim, Sol. Energy Mater. Sol. Cells 95 (2011) 344–348.
[23] Z.S. Wang, H. Kawauchi, T. Kashima, H. Arakawa, Coord. Chem. Rev. 248 (2004) 1381–1389.
[24] A.O.T. Patrocínio, L.G. Paterno, N.Y. Murakamilha, J. Photochem. Photobiol. A: Chem. 205 (2009) 23–27.
[25] J.B. Xia, N. Masaki, K.J. Jiang, S. Yanagida, Chem. Commun. (2007) 138–140.
[26] J.B. Xia, N. Masaki, K. Jiang, S. Yanagida, J. Phys. Chem. B 110 (2006) 25222–25228.
[27] J.B. Xia, N. Masaki, K.J. Jiang, S. Yanagida, J. Phys. Chem. C 111 (2007) 8092–8097.
[28] J.B. Xia, N. Masaki, K.J. Jiang, S. Yanagida, J. Photochem. Photobiol. A: Chem. 188 (2007) 120–127.
[29] M. Guo, P. Diao, X. Wang, S. Cai, J. Solid State Chem. 178 (2005) 3210–3215.
[30] X.M. Liu, X.H. Sun, Q.D. Tai, H. Hu, B.L. Chen, N. Huang, B. Sebo, X.Z. Zhao, J. Power Sources 196 (2011) 475–481.
[31] X.M. Liu, X.H. Sun, Q.D. Tai, H. Hu, B.L. Chen, N. Huang, B. Sebo, X.Z. Zhao, J. Alloys Compd., doi:10.1016/j.jallcom.2011.07.018, in press.
[32] A. Burke, S. Ito, H. Snaith, U. Bach, J. Kwiatkowski, M. Grätzel, Nano Lett. 8 (2008) 977–981.
[33] P. Cameron, L. Peter, J. Phys. Chem. B 107 (2003) 14394–14400.
[34] B. Peng, G. Jungmann, C. Jäger, D. Haarer, H.W. Schmidt, M. Thelakkat, Coord. Chem. Rev. 248 (2004) 1479–1489.
[35] H. Chang, K.C. Cho, C.G. Kuo, M.J. Kao, K.D. Huang, K.H. Chu, X.P. Lin, J. Alloys Compd. 509S (2011) S486–S489.
[36] S.R. Kim, M.K. Parvez, M. Chhowalla, Chem. Phys. Lett. 483 (2009) 124–127.
[37] J. Zhang, W.X. Que, Q.Y. Jia, P. Zhong, Y.L. Liao, X.D. Ye, Y.C. Ding, J. Alloys Compd. 509 (2011) 7421–7426.
[38] P. Zhong, W.X. Que, J. Zhang, Q.Y. Jia, W.J. Wang, Y.L. Liao, X. Hu, J. Alloys Compd. 509 (2011) 7808–7813.
[39] Q.H. Zhang, L. Gao, J. Eur. Ceram. Soc. 26 (2006) 1535–1545.
[40] S. Li, Y.G. Li, H.Z. Wang, W.G. Fan, Q.H. Zhang, Eur. J. Inorg. Chem. 27 (2009) 4078–4084.
[41] J.T. Jiu, S.J. Isoda, F.M. Wang, M. Adachi, J. Phys. Chem. B 110 (2006) 2087–2092.
[42] M. Adachi, Y. Murata, J. Takao, J. Jiu, M. Sakamoto, F. Wang, J. Am. Chem. Soc. 126 (2004) 14943–14949.
[43] M. Thelakkat, C. Schmitz, H.W. Schmidt, Adv. Mater. 14 (2002) 577–581.
[44] C.J. Brinker, F. Arendse, P. Comte, M. Jirousek, F. Lenzmann, V. Shklover, M. Grätzel, J. Am. Ceram. Soc. 80 (1997) 3157–3171.
[45] H. Yu, S.Q. Zhang, H.J. Zhao, B.F. Xue, P.R. Liu, G. Will, J. Phys. Chem. C 113 (2009) 16277–16282.